Available online at www.sciencedirect.com
SCIENCE DIRECT
Thin Solid Films 503 (2006) 29 – 39
thin solid films
www.elsevier.com/locate/tsf

Study of physical and photocatalytic properties of titanium dioxide thin films prepared from complex precursors by chemical vapour deposition

V.G. Bessergenev [a,*], R.J.F. Pereira [a,1], M.C. Mateus [a,2], I.V. Khmelinskii [a,3], D.A. Vasconcelos [a,1], R. Nicula [b,4], E. Burkel [b,5], A.M. Botelho do Rego [c,6], A.I. Saprykin [d]

[a] *Universidade do Algarve, FCT, Campus de Gambelas, 8005-139 Faro, Portugal*
[b] *University of Rostock, FB Physik, August-Bebel-Str. 55, 18055 Rostock, Germany*
[c] *Centro de Química-Física Molecular, Complexo Interdisciplinar, IST, 1049-001 Lisboa, Portugal*
[d] *Institute of Inorganic Chemistry, Russian Academy of Sciences, 630090 Novosibirsk, Lavrentiev Av. 3, Russia*

Received 27 June 2005; accepted 9 October 2005
Available online 28 November 2005

Abstract

Titanium dioxide (TiO_2) thin films were prepared using Titanium [bis(dipiraloymethanate) diisopropoxide] ($Ti(dpm)_2(OPr^i)_2$) and Titanium isopropoxide ($Ti(OPr^i)_4$) complex compound precursors by Chemical Vapour Deposition (CVD) and photo-assisted CVD. Structural information on TiO_2 thin films was obtained in synchrotron radiation experiments: high-resolution Grazing Incidence X-ray Diffraction (GIXRD) and $\theta-2\theta$ XRD experiments were performed on the high-resolution powder diffractometer at the Hamburg Synchrotron Laboratory. Chemical composition of thin films was studied by high-resolution Laser Ionization Mass Spectrometry technique, surface composition by X-ray Photoelectron Spectroscopy, and surface morphology by Atomic Force Microscopy. Photocatalytic activity of TiO_2 thin films was studied using a photocatalytic reactor. The fungicide Fenarimol was chosen as chemical indicator and its degradation kinetics was followed by High Performance Liquid Chromatography.

Keywords: Thin films; Titanium dioxide; CVD; Photocatalysis

1. Introduction

Titanium dioxide (TiO_2) has attracted significant attention of researchers because of many interesting physical properties that make it suitable for a variety of applications. For instance, its high dielectric constant gives it a potential as an insulator for capacitors for Dynamic Random Access Memory devices. TiO_2 has high corrosion resistance and chemical stability and an excellent optical transparency in the visible and near-infrared regions as well as high refractive index that makes it useful for anti-reflection coatings in optical devices. Since the discovery of photocatalytic splitting of water on TiO_2 electrodes [1], efforts were devoted to the development of efficient water and air purification technologies, based on TiO_2 photocatalysis. Such a treatment typically reduces toxic organic compounds to non-toxic inorganic compounds, such as carbon dioxide, water, ammonium or nitrates, and chloride ions.

A number of techniques, such as spray pyrolysis [2,3], sol-gel method [4,5], sputtering [6,7], solvothermal method [8], pulsed laser deposition [9], atomic layer deposition [10], Chemical Vapour Deposition (CVD) [11–15] and photo-assisted CVD [16] have been used to deposit TiO_2 thin films.

Each of the techniques for the TiO_2 thin film preparation has its own advantages and disadvantages, and it remains unclear at present as to which of these will eventually prove to be the most

* Corresponding author. Tel.: +351 289 800 900x7613; fax: +351 289 819 403.
E-mail addresses: vbess@ualg.pt, as3545561@sapo.pt (V.G. Bessergenev), rjper@ualg.pt (R.J.F. Pereira), mcmateus@ualg.pt (M.C. Mateus), ikhmelin@ualg.pt (I.V. Khmelinskii), duartemv@yahoo.com (D.A. Vasconcelos), radu-christian.nicula@uni-rostock.de (R. Nicula), eberhard.burkel@uni-rostock.de (E. Burkel), amrego@ist.utl.pt (A.M. Botelho do Rego), saprykin@che.nsk.su (A.I. Saprykin).
[1] Tel.: +351 289 800 900x7472.
[2] Tel.: +351 289 800 900x7644.
[3] Tel.: +351 289 800 900x7640.
[4] Tel.: +49 381 498 6863.
[5] Tel.: +49 381 498 6860.
[6] Tel.: +351 218 419 255; fax: +351 218 464 455.

0040-6090/$ - see front matter © 2005 Elsevier B.V. All rights reserved.
doi:10.1016/j.tsf.2005.10.046

cost–quality effective. However, some features of the CVD synthesis, such as its flexibility as regards the shape of the substrate, including the capability to create films on the inner surface of pipes and on flexible substrates; compatibility with lithographic methods; high quality of the prepared thin films and their good adhesion, make the CVD technique one of the most relevant for practical applications. It also should be mentioned that Atmospheric Pressure CVD is entirely compatible with the standard glass fabrication processes. Presently we pay special attention to the capability, by choosing an appropriate precursor, to produce either anatase or rutile crystal modification of TiO_2 thin films. Such a capability is useful for practical applications in photocatalysis and microelectronics. Additionally, we propose a method of lowering the synthesis temperature by use of UV-radiation from, for example, a standard mercury UV lamp, which can also be a valuable technological resource allowing to accommodate a wider range of substrates.

In spite of large efforts that have been aimed at studying both the solid state interfacial processes and the near-surface chemistry, there is no clear understanding of the mechanisms of decomposition of organic compounds. Therefore, we will first specifically concern ourselves with the properties of the TiO_2 thin film photocatalyst, setting aside the near surface chemistry that can be individual for each organic compound. There is no common standard developed for comparing photocatalytic activity, which makes it difficult to compare the films prepared by different methods and to optimise the photocatalyst preparation procedures. Recently, a technique has been proposed for quality comparison of the thin film photocatalysts prepared by different methods, which uses the photocurrent images [17]. Indeed, a correlation between photocurrent and photocatalytic activity had been demonstrated in certain cases; in some films, however, an increase in photocurrent is not accompanied by an increase in the contaminant degradation rate [12]. Therefore, other relevant parameters apart from the photocurrent should exert a strong influence on the photocatalytic activity. The photocatalytic activity depends strongly on the surface redox potential and the lifetime of the photogenerated electron-hole pairs. Titanium dioxide exists in three different crystalline phases: anatase, rutile and brookite [18]. Anatase was found to be more active photocatalytically than rutile [19]. This enhanced photoactivity is attributed to the larger bandgap existing in this crystalline phase, which generally leads to an increase of both the surface redox potential and the charge carrier lifetime. Photocatalytic activity is also very sensitive to the surface charge stabilisation attributed to variations of crystalline orientation. Recently a new technique for characterising photocatalytic activity of thin films that employed a pulsed laser excitation with subsequent registration of the carrier lifetime without metal contacts has been reported [20]. The method was used to study highly oriented TiO_2 thin films in the anatase and rutile forms.

In practice, however, resulting from the need to establish a common point of reference, the photocatalytic activities are frequently compared to that of the Degussa P25 TiO_2 powder, which is a mixture containing of 80% of the anatase and 20% of the rutile phases.

The existence of two different crystalline forms should allow optimisation of the titanium dioxide properties for applications such as dielectrics for thin film capacitors or as photocatalysts for water and air purification. Indeed, the low values of photocurrent due to electron-hole trapping by impurities should limit the usage of rutile in the photocatalysis. Instead, this modification should be more useful in applications such as dielectric ceramics.

Presently, we have used the CVD techniques to prepare titania thin films from two different precursors, and comprehensively investigated their chemical composition, crystal structure, surface composition, and photocatalytic activity. The photocatalytic activity was compared to that of the Degussa P25 powder.

2. Experimental details

2.1. Materials

The TiO_2 thin films were prepared using titanium[(dipiraloymethanate) diisopropoxide] $Ti(dpm)_2(OPr^i)_2$ (precursor A) and titanium[isopropoxide] $Ti(OPr^i)_4$ (precursor B) (dpm=2,2,6,6-tetramethylheptane-3,5-dione, Pr^i=isopropyl) as the complex compound precursor materials. Initially the precursor A was purchased from the Institute of Inorganic Chemistry of the Siberian Branch of Russian Academy of Sciences. It later became commercially available at Aldrich Chemicals (UK). The A-type precursors purchased from both of the above-mentioned sources demonstrated identical results. Precursor B was purchased from Aldrich Chemicals. All precursors were used as received. Precursor A is a solid powder and precursor B is a liquid. Their structural formulas are presented in the Fig. 1. The thermal properties of the precursors A and B are described in Refs. [21,22], respectively.

To study the utility of photo-activated processes during a thin film synthesis (photo assisted CVD), absorption spectra of the precursor vapours were investigated. A photo assisted CVD process of thin film synthesis using $Ti(OPr^i)_4$ as precursor and krypton–chlorine (KrCl*, λ=222 nm) excimer lamp as UV radiation source had been proposed recently [16]. However, the absorption spectrum of this precursor remained unknown. The absorption spectra of the vapours of the $Ti(OPr^i)_4$ and $Ti(dpm)_2(OPr^i)_2$ precursors are shown on Figs. 2 and 3, respectively, and were recorded on a CINTRA 40 UV-VIS spectrophotometer.

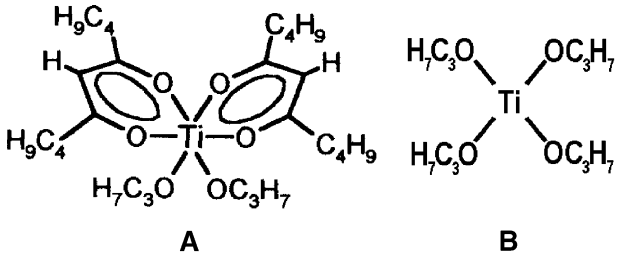

Fig. 1. Structural formulas for $Ti(dpm)_2(OPr^i)_2$ (precursor A, left) and $Ti(OPr^i)_4$ (precursor B, right).

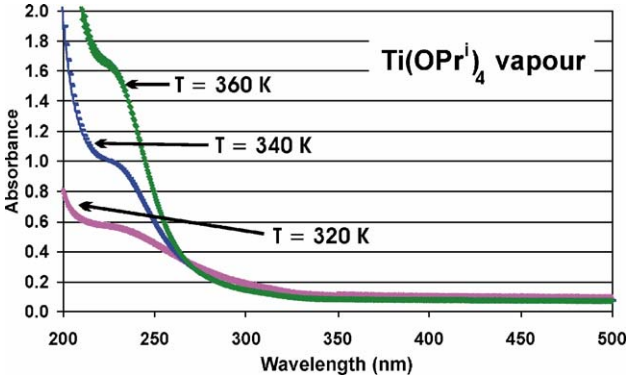

Fig. 2. The absorption spectra of Ti(dpm)$_2$(OPr^i)$_2$ (precursor A) vapours at different temperatures.

Comparing Figs. 2 and 3, we note that the light absorption by the vapours of the precursor A starts at the wavelength of ca. 380 nm. This value is much higher than 250 nm, where the precursor B starts to absorb. Using this knowledge, the photo assisted CVD process was implemented using two high-pressure mercury lamps. The mercury lamps were placed outside the vacuum chamber and the deposition substrates were illuminated through fused silica windows at a distance of 50 cm, without any optical elements. Estimates show that only a small part of the Hg lamp radiation was absorbed by the precursor vapour in this photo-assisted process. Nevertheless, the synthesis temperature could be reduced to 360 °C as compared to 420 °C required for the conventional CVD deposition process.

2.2. TiO_2 film preparation

The synthesis of titanium dioxide thin films by low pressure CVD has been described in detail elsewhere [14,15]. Briefly, the TiO_2 films were obtained in a standard vacuum apparatus with a turbo-molecular pump ALCATEL TMP 5400 CP (pumping capacity ~0.4 m^3/s at $P<10^{-2}$ Pa) producing vacuum down to 5×10^{-5} Pa (5×10^{-7} mbar). Vaporisation was conducted from an open surface evaporator. The temperature of the vapour source was varied in the 90–210 °C range, and the substrate temperature was stabilised in 450–600 °C range. Different types of rectangular or round glass and fused silica plates of 78.5 cm^2 maximum area were used as substrates. All substrates were cleaned carefully right before loading, using the following procedure. First, the substrates were cleaned in water using a detergent and then rinsed in distilled water. Second, the substrates were immersed in sulphuric acid (~95%) for about 24 h, then rinsed by distilled water and washed with acetone and finally dried in a flux of filtered air.

The film thickness ranged from 30 to 2000 nm and was measured by weight with an expected error of 10%. The growth rate could be varied from several nanometres to several tens of nanometres per minute.

The CVD apparatus [14,15] was presently modified by addition of gas supply lines that allow to introduce inert gases (Ar, He) and oxygen into the chamber. The pressure in the CVD chamber was varied between 1.2×10^{-2} Pa and 10 Pa (1.2×10^{-4} and 0.1 mbar), with the system working either in the molecular vapour stream or gas flow regime. The pressure of the volatile precursor decomposition products determined the available lower pressure limit. Some of the film preparation conditions are summarised in the Table 1.

2.3. Methods

Structural information on as-prepared TiO_2 thin films was obtained from the synchrotron radiation experiments. High-resolution grazing-incidence X-ray diffraction (GIXRD) as well as $\theta-2\theta$ experiments were performed at the high-resolution powder diffractometer at the DESY/HASYLAB synchrotron radiation laboratory, using grazing-incidence angles α_i between 0.9° and 1.0° and synchrotron radiation wavelength of 0.11315 nm. Thin films deposited on either glass or fused silica substrates were analysed.

The trace analysis of the TiO_2 films was performed by laser ionization mass spectrometry (LIMS). A double-focusing mass spectrometer with Mattauch–Herzog geometry and laser plasma ion source (EMAL-2) was used. The energy output of Nd-YAG laser (wavelength of 1064 nm), its pulse duration, repetition rate and diameter of laser spot on the sample surface were adjusted to evaporate and ionize the deposited films only. The glass substrates are transparent to the Nd-YAG laser radiation and suffered almost no laser damage. At the chosen radiation power density (~1×10^9 W/cm^2) the measured concentration of Si (the main component of the substrate) never exceeded 10^{-2} at.%. Step motors provided for scanning of the sample in two directions (X–Y). The area of the analyzed sample surface was about 0.5 cm^2. The concentrations of impurities were evaluated with respect to Ti (matrix element of the deposited layer) as the internal standard.

The TiO_2 films were analysed by X-ray Photoelectron Spectroscopy (XPS) using XSAM800 (KRATOS) X-Ray Spectrometer operated in the fixed analyser transmission mode. A Mg K_α (1253.7 eV) X-ray source was used. The analyser was operated at 20 eV pass energy both for detailed and survey spectra. All the binding energies were referenced to the C 1s peak at 285.0 eV or O 1s peak at 529.9 eV. Shirley backgrounds were subtracted and Voigt profiles (Gaussian and Lorentzian products) were used for fitting purposes.

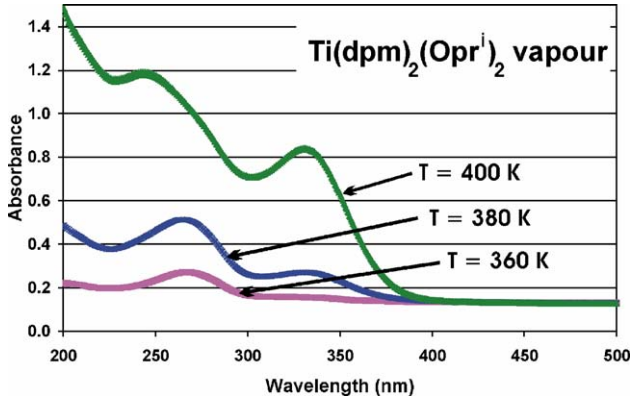

Fig. 3. The absorption spectra of Ti(OPr^i)$_4$ (precursor B) vapours at different temperatures.

Table 1
Typical conditions of TiO_2 thin film synthesis

Sample	Precursor	Substrate	Thickness (nm)	T_{Sub} (°C)	P max. × 10^2 (Pa)	R (MΩ)	Flux, % Ar/O_2
1	A	Glass	250	540	1.2×10^{-4}		Vacuum
2		Quartz	250	450	1.4×10^{-4}		Vacuum
3		Quartz	150	500	2.4×10^{-5}		Vacuum
4		Quartz	295	550	1.6×10^{-4}		Vacuum
5		Quartz	300	600	4.0×10^{-4}		Vacuum
6		Quartz	255	450	5.7×10^{-2}	>200	50/100
7		Quartz	575	500	1.8×10^{-1}	>200	50/100
8		Quartz	655	500	1.8×10^{-1}	>200	50/100
9		Glass	150	450	1.4×10^{-1}	>200	50/100
10		Glass	215	450	1.4×10^{-1}	>200	50/100
11		Glass	465	470	1.2×10^{-1}		50/100
12		Glass	300	470	1.2×10^{-1}		50/100
13_UV		Quartz	45	400	1.5×10^{-5}		Vacuum
14_UV		Glass	60	400	1.2×10^{-5}		Vacuum
15		Glass	85	420	1.4×10^{-4}		Vacuum
16		Glass	40	450	7.8×10^{-5}		Vacuum
17		Glass	110	450	2.8×10^{-4}		Vacuum
18		Ceramic	165	465	1.1×10^{-4}		Vacuum
19		Ceramic	360	480	2.8×10^{-5}		Vacuum
20		Ceramic	140	520	6.4×10^{-4}		Vacuum
21		Ceramic	220	450	1.2×10^{-4}		Vacuum
22_UV		Quartz	45	400	1.5×10^{-5}		Vacuum
23	B	Quartz	55	450	2.1×10^{-1}	>200	100/0
24		Quartz	485	450	6.4×10^{-5}	>200	Vacuum
25		Glass	345	450	6.4×10^{-5}	0.3–6.6	Vacuum
26		Glass	250	400	1.2×10^{-4}		Vacuum
27		Glass	1475	450	2.8×10^{-4}	0.06–0.5	Vacuum
28		Glass	360	375	4.0×10^{-4}	0.05–0.9	Vacuum
29		Glass	760	360	5.1×10^{-4}	0.03–0.3	Vacuum
30		Glass	1745	400	2.1×10^{-1}	>200	50/100
31		Glass	970	450	3.7×10^{-1}	>200	50/100

100% of gas flux corresponds to 25 ml_n/min (ml_n—millilitres at normal atmospheric pressure).

Atomic Force Microscopy (AFM) measurements were performed on a Nanoscope-2000 AFM system (Digital Instruments) at room temperature and atmospheric pressure. SiN uncoated AFM probes were used (Veecol, Inc.), with the following geometric parameters: 35° angle, 20 nm nominal tip radius, and 60 nm maximum tip radius. Tapping mode was employed with the resolution of 256×256 samples and 3.13 Hz scan rate.

2.4. Photocatalytic activity measurements

The layout of the photoreactor apparatus is described in detail in Ref. [15]. Briefly, the volume of irradiated solution was of 7.9 mL at 1 mm optical thickness. A 200 W Xenon lamp was used as an UV light source and a water filter with fused silica windows was used in order to avoid excessive heating of the solution. The photocatalytic process in water requires the presence of O_2 as electron acceptor, thus a low (ca. 3 mL/min) continuous flow of air was injected by means of an air pump.

Fenarimol (Riedel, 99.7%) 5 mg/L solutions were prepared in bidistilled water. The Fenarimol solutions were left in contact with the reactor cell about 12 h in the dark before irradiation in order to achieve the adsorption equilibrium of the pesticide between the solution and the cell surfaces. This step was necessary because of low pesticide solubility and large surface area of the reactor cell.

During irradiation, 100 μL samples were taken every 0.5 or 1 h, and immediately analysed on a High Performance Liquid Chromatography (HPLC) system (Merck-Hitachi 655A-11 system with 655A-22 UV detector) in the following experimental conditions: LichroCART 125-4 column: Lichrospher 100 RP-18, 5 μm; eluent: acetonitrile (Merck Lichrosolv) 65%, bidistilled water 35%; 1.1 mL/min flow; UV detection at 220 nm.

The total irradiation time was between 3 and 5 h for each sample. To compare the reaction rates obtained for the thin films, commercial TiO_2 P25 powder (Degussa) with identical amount by weight (7 mg) was deposited on fused silica substrates by evaporation from a TiO_2 aqueous suspension and tested under identical experimental conditions.

3. Results and discussion

3.1. Crystal structure of the thin films

The structural phases that may be formed in titanium dioxide samples are the amorphous phase, the metastable crystalline forms brookite and anatase, and the high-temperature stable phase rutile [18]. It should be noted that

other oxide phases, Ti_2O, TiO, Ti_2O_3, Ti_3O_5 and Ti_nO_{2n-1} ($n=4$, ..., 10) may also appear at low oxygen concentrations.

The transition from the amorphous to the anatase form usually requires temperatures close to 300 °C. In nanocrystalline TiO_2 powders, the irreversible anatase→rutile phase transition occurs between 600 and 800 °C [23]. In bulk specimens, the anatase-to-rutile transition occurs at temperatures above 800 °C.

GIXRD studies of crystal structure for samples prepared from precursor A as well as thermal decomposition mass spectrometry studies for precursor A in vacuum and in the presence of oxygen were reported in detail earlier [14,15]. In the present work, thin films prepared from precursors A and B in vacuum and in Argon/Oxygen gas flux were studied by X-ray diffraction (Figs. 4 and 5).

As illustrated in Figs. 4 and 5, a significant difference between films deposited from precursors A and B is that for precursor A polycrystalline rutile films were obtained, while for precursor B the films consist of polycrystalline anatase. It is important to emphasize that all the synthesis conditions for the films derived from both precursors were very similar (see Table 1) and the resulting crystal structure was independent on the substrate (glass, fused silica, or Si wafer). Thus the choice of the precursor can be used to control the form of the titanium dioxide produced.

We are unable to rigorously explain these experimental results, either theoretically or by modelling, due to the lack of knowledge on the structure and geometry of the principal molecular fragments of these precursors participating in the thin film. Moreover, the information about the molecular geometry of the precursors A and B and their eventual clusters in the vapour phase is also missing. The crystal structures of these precursors are equally unknown, because of difficulties in growing single crystals for the precursor A and the liquid phase state of the precursor B in normal conditions. It has been shown [21] by mass spectroscopic analysis of the decomposition fragments of precursor A that its decomposition pathways in vacuum and in the presence of oxygen are different. However, the samples prepared from the precursor A either in vacuum or in the Ar/O_2 atmosphere always had the rutile crystal form. Therefore, considering the structural

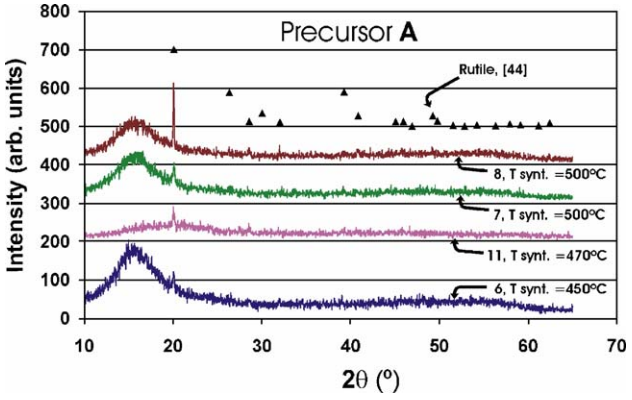

Fig. 4. X-ray diffraction patterns for the samples prepared from precursor A (▲)–JCPDS data, Card 89–4920 [44].

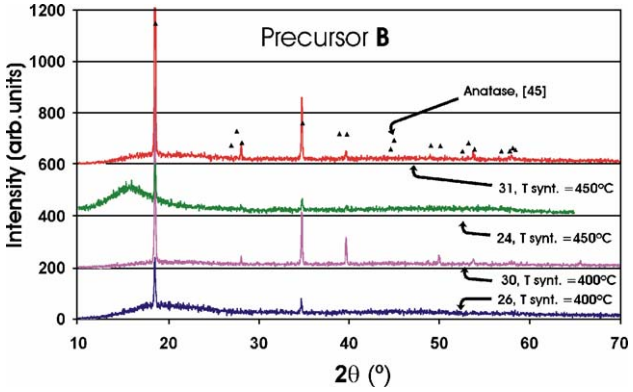

Fig. 5. X-ray diffraction patterns for the samples prepared from precursor B (▲)–JCPDS data, Card 89–421 [45].

formulas only (Fig. 1), we note that the molecular structure of the precursor B is more symmetrical then that of the precursor A. Additionally, the intermolecular interactions are weaker in B, which, contrary to A, stays liquid in normal conditions. This could be the reason for the metastable anatase phase to be produced from the precursor B. This idea is supported by the fact that the structure initially formed in the sol–gel powder is amorphous, and may be subsequently transformed into anatase and then into rutile by annealing [23].

At higher processing temperatures the intensities of the diffraction peaks increase for both precursors and for the same type of substrate. Note, for example, that the peak intensities for Sample 31 are much higher although the Sample 30 film is thicker. Both samples were deposited from the precursor B on glass substrates. Higher synthesis temperatures lead to formation of coarser microstructures. Additionally, the specimens may contain a certain amount of amorphous TiO_2, which cannot be detected by X-ray diffraction for films deposited on glass substrates. In fact, it

Table 2
The results of mass-spectrometry analysis*

Impurity	Sample 1	Sample 2	Sample 3	Sample 4	Sample 5
C	$\approx 5\times10^{-1}$	$\approx 5\times10^{-1}$	$\approx 5\times10^{-1}$	$\approx 5\times10^{-1}$	$\approx 5\times10^{-1}$
N	$\leq 2\times10^{-2}$	$\leq 2\times10^{-2}$	$\leq 2\times10^{-2}$	$\leq 4\times10^{-2}$	$\leq 4\times10^{-2}$
Na**	$<2\times10^{-1}$	$<2\times10^{-1}$	$<2\times10^{-1}$	$<2\times10^{-1}$	$<2\times10^{-1}$
Mg**	$<1\times10^{-2}$	$<1\times10^{-2}$	$<1\times10^{-2}$	$<1\times10^{-2}$	$<1\times10^{-2}$
Al	5×10^{-3}	3×10^{-2}	7×10^{-3}	4×10^{-3}	1×10^{-2}
P	3×10^{-3}	3×10^{-3}	3×10^{-3}	1×10^{-3}	2×10^{-3}
Cl	1×10^{-2}	5×10^{-2}	1×10^{-2}	7×10^{-3}	4×10^{-2}
K	2×10^{-1}	4×10^{-2}	2×10^{-2}	1×10^{-2}	2×10^{-2}
Ca	7×10^{-2}	1×10^{-1}	3×10^{-2}	8×10^{-2}	8×10^{-2}
Cr	1×10^{-3}	7×10^{-4}	5×10^{-4}	1×10^{-3}	5×10^{-3}
Mn	6×10^{-4}	1×10^{-3}	9×10^{-4}	3×10^{-4}	1×10^{-3}
Fe	1×10^{-2}	3×10^{-1}	2×10^{-1}	1×10^{-1}	1×10^{-1}
Co	n/f(6×10^{-4})	n/f(6×10^{-4})	n/f(6×10^{-4})	n/f(6×10^{-4})	n/f(6×10^{-4})
Ni	2×10^{-3}	8×10^{-4}	n/f(6×10^{-4})	n/f(6×10^{-4})	5×10^{-3}
Cu	3×10^{-3}	4×10^{-1}	2×10^{-1}	1×10^{-1}	1×10^{-1}
Zn	3×10^{-2}	4×10^{-2}	1×10^{-1}	2×10^{-2}	5×10^{-2}

The values are given in at.%. n/d—not detected, the detectability threshold is given in brackets.
* Standard deviation $s_r=0.15-0.25$.
** Detectability limited by the superimposed signal of doubly charged ions of the matrix.

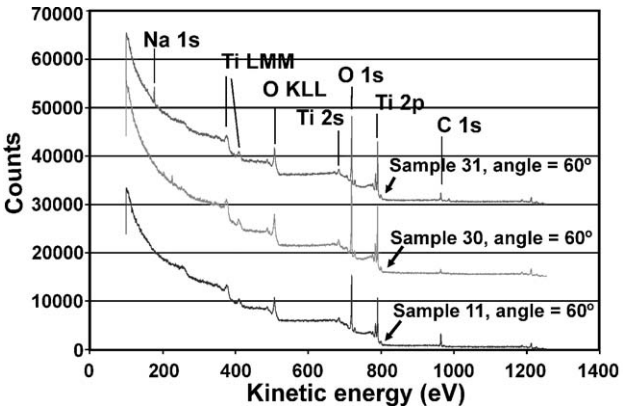

Fig. 6. XPS survey spectra for the surface of TiO_2 films prepared from the precursors A and B.

was impossible to observe the diffraction pattern peaks by the $\theta-2\theta$ method for the samples prepared by photo assisted CVD, Sample 13_UV and Sample 14_UV (see Table 1) at T_{synt}=400 and 350 °C.

3.2. Trace mass spectrometric analysis

So far, little is known about the real composition of TiO_2 thin films used for photocatalytic activity studies, probably because of the complexity of such studies. However, one of the factors that have a strong influence on the photocatalytic activity can be a contamination of TiO_2 thin films by the dopants. Average concentrations of impurities in the TiO_2 films were obtained by laser ionization mass spectrometry. The results of LIMS analysis are shown at Table 2. All the analyzed samples were synthesized on fused silica substrates, so that the presence of Na and Ca is relatively small and should be related to ceramic parts used in the construction of the substrate heater. Large sample to sample variability is observed for contamination by Fe, Cu, K and Zn. Because of the absence of a representative statistic (only five samples were studied by LIMS) the presence of some impurities, such as K for the Sample 1 and Zn for Sample 3 is yet unclear and probably occasional. However, we can still obtain a clear notion about the level of different elements present in the samples, as shown in Table 2. The Fe and Cu impurities probably originate

Table 3
Composition (atomic percentage, at.%) of TiO_2 films and binding energies according to XPS analyses

Attribution	Sample 1	Sample 2	Sample 3	Sample 4	Sample 7	Sample 11	Sample 30	Sample 31
Angle= 0°								
Ti 2p $_{3/2}$	8.6	4.1	8.4	8.1	8.5	11.2	14.1	14.0
Ti 2p $_{1/2}$	4.3	1.9	4.0	3.9	4.2	5.4	6.8	6.7
Metallic oxygen	26.1	16.9	29.9	28.1	30.5	41.1	53.0	51.3
Organic oxygen	5.6	9.9	6.4	4.6	5.2	5.0	5.9	4.0
Adsorbed oxygen	7.6	3.5	2.4	14.4	9.1	2.1	4.3	3.7
Hydroxyl oxygen	1.4	0.52		2.2	1.5	0.6	1.2	
Carbon total	39.0	54.9	42.8	30.4	35.5	34.6	14.8	20.3
Aliphatic carbon				2.2	1.5	31.0	9.6	15.5
C–O	3.9	3.6	3.1	1.6	3.4	1.3	2.6	1.5
C=O	3.4	4.8	3.0	6.7	2.2	2.3	2.5	3.4
Ti1/Ti2*	2.0	2.2	2.1	2.1	2.0	2.1	2.0	2.1
Metallic oxygen/Ti	TiO2.0	TiO2.9	TiO2.4	TiO2.3	TiO2.4	TiO2.5	TiO2.5	TiO2.5
Angle= 60°								
Ti 2p$_{3/2}$	8.2	5.5	8.5	5.1	12.1	11.5	15	14.1
Ti 2p$_{1/2}$	3.8	2.7	3.9	2.4	5.9	5.6	7.5	7.1
Metallic oxygen	28.4	20.8	30.3	18.2	37.9	41.7	54.7	49.4
Organic oxygen	6.1	8.3	9.9	3.2	10.3	3.8	4.7	2.3
Adsorbed oxygen	6.2	6.0	5.4	17.5	9.4	2.9	4.3	4.6
Hydroxyl oxygen	1.0	2.6						
Carbon total	39.4	45.4	36.9	40.9	23.4	34.1	12.5	22.6
Aliphatic carbon				2.2	1.1	30.5	8.2	18.4
C–O	3.4	4.7	2.7	1.59	2.0	1.3	2.3	1.1
C=O	3.6	4	2.5	9.1	1.6	2.3	2.0	3.1
Ti1/Ti2*	2.2	2.0	2.2	2.1	2.1	2.0	2.1	2.0
Metallic oxygen/Ti	TiO2.4	TiO2.5	TiO2.4	TiO2.4	TiO2.1	TiO2.4	TiO2.4	TiO2.3
Binding energy, eV (angle= 0°)								
Ti 2p $_{3/2}$	458.6	458.5	458.6	458.6	458.7	458.6	458.6	458.6
Ti 2p $_{1/2}$	464.3	464.2	464.2	464.3	464.4	464.2	464.3	464.2
Metallic oxygen	529.9	529.9	529.9	529.9	529.9	529.9	529.9	529.9
Organic oxygen	531.6	531.7	531.7	531.0	531.5	531.7	531.6	531.6
Adsorbed oxygen	532.5	532.6	532.4	532.1	532.4	532.39	532.4	532.4
Hydroxyl oxygen	533.9	533.6	533.5					
Aliphatic carbon	285.1	285.1	284.9	284.7	285.0	284.7	284.7	285.0
C–O	287.2	287.0	286.8	286.8	287.5	286.82	286.3	286.8
C=O	288.8	288.8	288.6	288.8	288.9	288.53	288.8	288.8

*Ti 2p$_{3/2}$/Ti 2p$_{1/2}$ theoretical value=2.

from the interaction of the precursor vapours with the metallic parts of the CVD apparatus. The presence of C at 5×10^{-1} at.% level can be attributed to the residual carbon deposited during the process of precursor decomposition.

3.3. XPS studies

Fig. 6 shows the XPS survey spectra taken at the surface of TiO_2 films prepared from precursors A and B. All the spectra were taken at the sample angles of 0° and 60° to document changes in the film composition at the sample surface. Fig. 6 shows that the films contain Ti, O and C. The relative contents of these elements and their binding energies are given in the Table 3.

The XPS results demonstrated that the samples 30 and 31 are slightly contaminated with sodium and zinc, respectively. The origin of sodium contamination comes from the glass substrate, as had been shown, for example, in Ref. [24]. However, the origin of zinc contamination is unclear. These samples were analysed by XPS after their photocatalytic activity studies were performed, thus the respective contamination may originate from the aqueous solutions that have been in contact with the sample surface. Comparing the mass spectrometry data with those of the XPS analysis, we note that a larger concentration of carbon is found on the surface compared to the bulk, indicating the redistribution of carbon during thin film growth. The strong and seemingly stochastic variations of the carbon contents at the very surface (as monitored by the XPS data taken at 0° and 60°, see Table 3) indicate that carbon is distributed extremely heterogeneously within the surface atomic layers, both laterally and vertically. These results, however, remain consistent with the mass-spectrometry results, which always produce the average carbon contents over the whole thickness of the film, which is ca. 1000 atomic layers, whereas XPS analyses the layer which is typically only 10 atomic layers. Several process parameters affect the surface contamination by carbon, including the synthesis temperature, the oxygen concentration in the vapour phase during film growth, the type of precursor, etc. The total carbon content as determined by XPS analysis is shown in the Fig. 7.

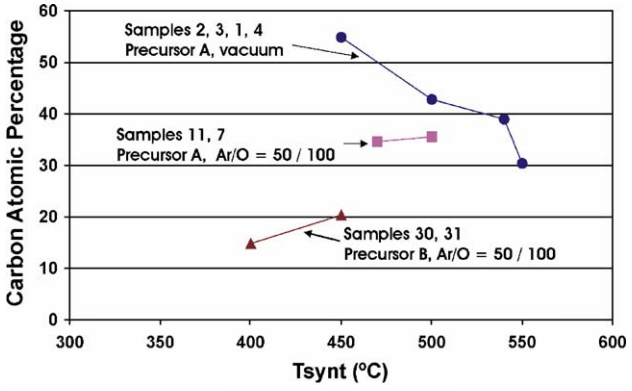

Fig. 7. Total carbon contents determined by XPS at different experimental synthesis conditions. Atmosphere: Ar/O=50/100 means 50% gas flux of argon and 100% gas flux of oxygen, 100% corresponds to 25 ml_n/min (ml_n—millilitres at normal atmospheric pressure).

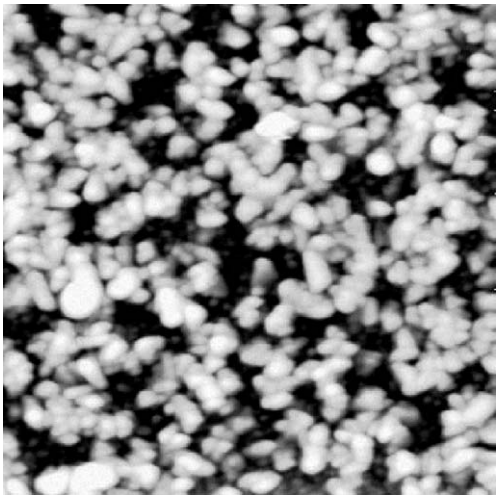

Fig. 8. This is an AFM image of the Sample 12: the field size is 2 μm by 2 μm; the shades of grey correspond to the vertical scale of the recording of 0 to 80 nm.

The total carbon content decreases with increasing process temperature for samples synthesised from precursor A in vacuum. The carbon content is also lower for samples prepared in the presence of oxygen under otherwise identical conditions, which may be explained in at least two different ways. First, as earlier shown by MS analysis of the precursor A decomposition products [21], the thermolysis mechanism on the heated surface in the isolated molecule approximation is different in vacuum and in oxygen. Second, the decomposition products will form gaseous CO and CO_2 much easier in presence of oxygen than in vacuum.

The total carbon content of samples prepared from precursor B in the presence of oxygen is even lower and increases with increasing processing temperature, which is probably related to a different kinetic mechanism of thin film growth. The latter hypothesis is supported by the fact that the crystal structures of films prepared from the two precursors are different.

3.4. AFM results

The AFM results demonstrated that the TiO_2 film samples have a porous polycrystalline structure, with a typical crystallite size of about 100 nm. The typical film thickness of about 500 nm suggests that the entire volume of the film should be accessible to the aqueous reactants. A typical micrograph is shown in Fig. 8.

3.5. Photocatalytic activity

The HPLC results of the photocatalytic activity studies are summarised in Table 4. The parameter that characterises the fungicide Fenarimol decomposition rate (k) is determined from the first-order reaction equation as $\ln(P_0/P_t)=k \times t$, P_0 and P_t being the initial and current concentrations of Fenarimol.

The photocatalytic activity of TiO_2 thin films was estimated not only by the decrease of Fenarimol chromatographic peak area but also by the decay of intermediate photoproducts,

Table 4
Results of photocatalytic activity studies

Sample	Precursor	T_{synt}, °C	Ar/O_2	K (h^{-1})	Photocatalytic effect
15[a]	A	420	Vacuum	0.53±0.03	Not observed
16[a]	A	450	Vacuum	0.53±0.04	Not observed
17[b]	A	450	Vacuum	0.39±0.01	Not observed
18[c]	A	400	Vacuum	0.49±0.01	Not observed
19[c]	A	450	Vacuum	0.31±0.02	Not observed
20[c]	A	520	Vacuum	0.11±0.01	Not observed
21[d]	A	450	Vacuum	0.41±0.02	Not observed*
22-UV[c,e]	A	400	Vacuum	0.36±0.05	Not observed
9[a]	A	450	50/100	0.36±0.03	Not observed
10[a]	A	450	50/100	0.34±0.01	Not observed
26[a]	B	400	Vacuum	0.85±0.02	Observed
27[a]	B	450	Vacuum	0.80±0.04	Observed
28[a]	B	375	Vacuum	0.99±0.04	Observed
29[a]	B	360	Vacuum	0.72±0.03	Observed
30[a]	B	400	50/100	0.96±0.01	Observed
Degussa powder P25[a]	Film obtained by evaporation of aqueous suspension with 7 mg of TiO_2 powder			5.2±0.4	Observed

[a]Deposition on ordinary glass. [b]Stripped glass. [c]Quartz. [d]Ceramic glass. [e]Film deposition assisted by UV light.
*The results of the first experiment using these conditions were not reproducible.

namely the photoproduct with m/z 328 [22,43]. This photoproduct is more stable to irradiation than Fenarimol when adsorbed on a glass or quartz surface. A first chromatographic peak appearing in the chromatograms (Fig. 9) corresponds to non-retained low molecular weight compounds. This peak increases with the degradation of Fenarimol itself as well as a consequence of degradation of all intermediate photodegradation products. Two concurrent degradation processes occur in the photoreactor, namely the direct photodegradation caused by the UV light absorbed directly by the test compound and the photocatalytic degradation. Therefore, the chemical stability of the intermediate photoproducts depends also on the photocatalytic activity of the TiO_2 thin films.

Typical chromatograms shown in Fig. 9 were obtained with two kinds of samples, Sample 10 (precursor A) and Sample 30 (precursor B), and also with the Degussa P25 powder. All samples were analysed using identical experimental conditions, clarifying the differences between Fenarimol degradation process induced by the samples prepared from two different precursors and the film prepared from an aqueous suspension of Degussa P25 powder. In spite of the Fenarimol degradation rate for Degussa powder film being markedly higher, the degradation process for Sample 30 follows an identical tendency.

The kinetics of Fenarimol decay and the kinetics of its intermediate photoproduct (m/z 328) formation for the thin films listed in Table 4 are shown in Fig. 10 (A) and (B), respectively. The abundances of Fenarimol and of its intermediate photoproduct is expressed here in terms of the respective chromatographic peak areas, which, for the same experimental conditions, are proportional to the chemical concentrations for each instant of analysis time.

Of all the films tested, the TiO_2 films prepared from the precursor B were the only samples to exhibit any photocatalytic activity. Indeed, for these samples the concentration of the intermediate photoproduct starts to decrease after about 1.5 h of irradiation. Besides, Fenarimol decay rate is also clearly improved for these samples.

There are different factors that can have a strong influence on the photocatalytic activity and should be taken into account when the photocatalytic activity of TiO_2 thin films is analysed. These are: the crystal modification, the bulk and surface chemical composition, and the effective surface area or the surface morphology. As it was shown by LIMS and XPS (Sections 3.2 and 3.3, respectively) the bulk carbon content is about 0.5 at.%, there also exist strong variations in the degree of surface carbon contamination. The difference in carbon content amounts to a factor of 2 (see Fig. 7) for the samples from precursor A (ca. 35 at.% of C) and precursor B (15–20 at.% of C) prepared in the Ar/O_2 atmosphere. The absence of photocatalytic activity for samples prepared from precursor A can only be explained supposing that there exists a threshold in the catalytic activity as a function of the degree of surface carbon contamination. It has been shown, however, that samples prepared via the sol–gel method [24–26] as well as via plasma source ion implantation method [27] with anatase

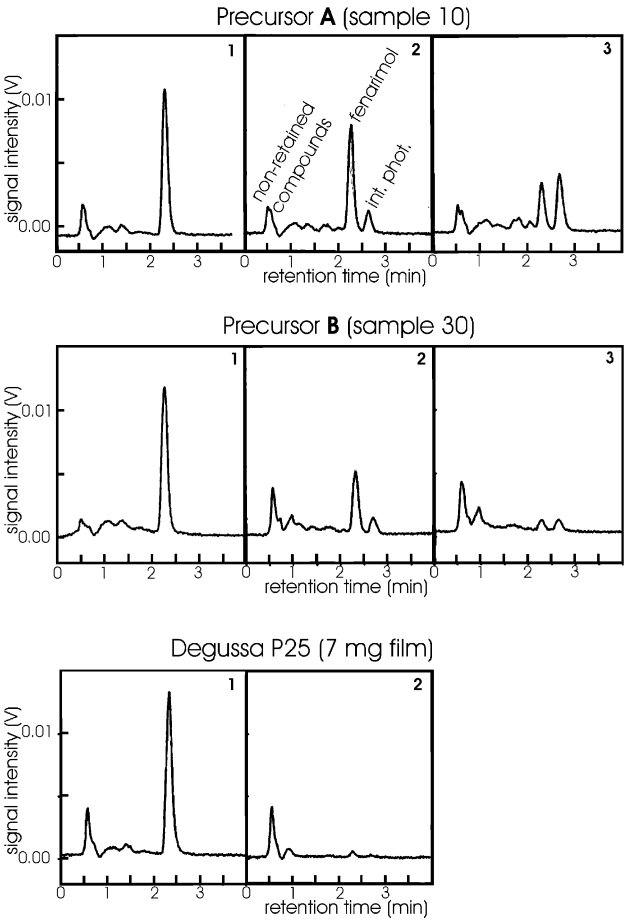

Fig. 9. Chromatograms of Fenarimol (5 mg/L aqueous solution) degradation for three TiO_2 thin films samples, after 1 and 3 h of UV irradiation. Notes for this figure: 1—Initial time; 2—After 1 h of irradiation; 3—After 3 h of irradiation.

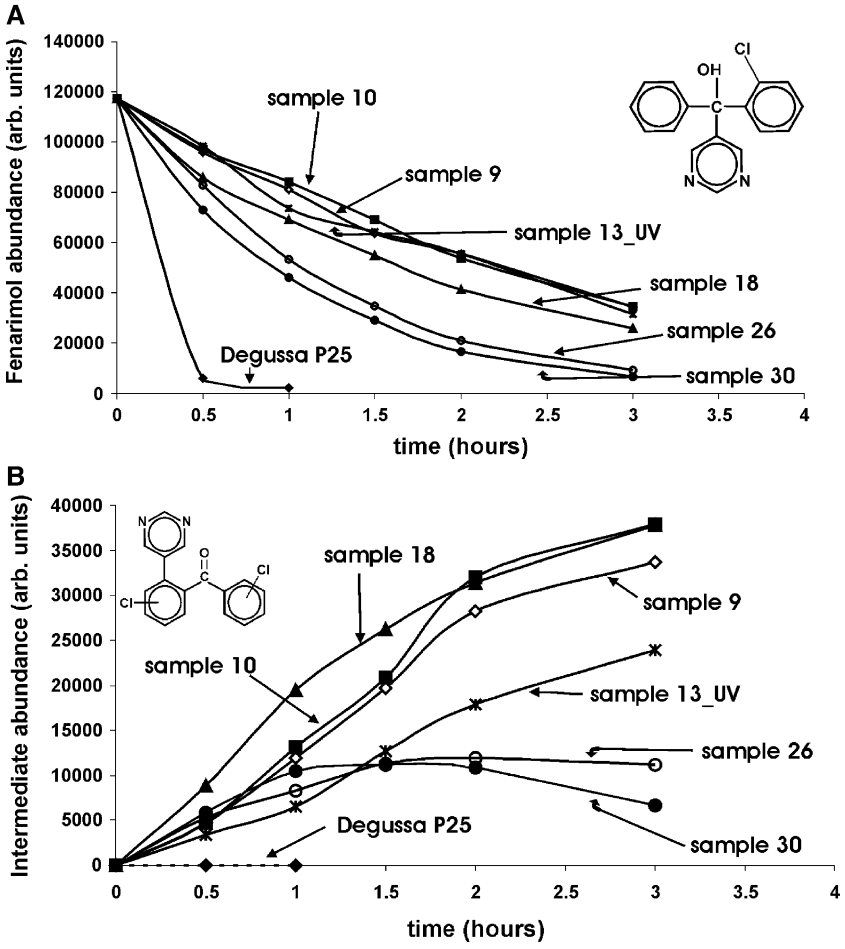

Fig. 10. Contents of Fenarimol (A) and intermediate photoproduct (B) in aqueous solutions, in function of time under UV illumination in contact with different TiO_2 thin films.

crystal modification are photocatalytically active at 9.6–14.9 at.% [24], at 20 at.% [27], and or even at 31–43 at.% [25,26] of surface carbon contamination (XPS data). The microscopic mechanism of the influence of the superficial and near-superficial carbon on the photocatalytic activity, which might involve electron-hole trapping, fast electron-hole recombination at the impurity, and the electron density redistribution, is yet unknown. Furthermore, in at least two cases carbon was reported as beneficial for the photocatalytic activity [28,29]. Therefore, the hypothesis of a carbon contamination threshold may be discarded.

The photocatalytic properties of TiO_2 thin films doped with metals have been discussed recently for Na (14.4 and 8.5 at.%) [24] Na (3.35 and 1.37 at.%) [26], Fe (0.76 at.%), Co (0.62 at.%), Ni (0.60 at.%), Mo (0.56 at.%), Nb (0.88 at.%), W (0.52 at.%) [30], V (3×10^{16} and 6×10^{16} ion/cm^2), Cr, Mn, Fe, [31], Sn (2×10^{13} ion/cm^2) [32] and Sn (2×10^{15} ion/cm^2) [33], Au (0.8 μg/cm^2) [34], Fe (2×10^{17} ion/cm^2) [35], Pt (4 wt.%) [36], and doped with nitrogen (the nitrogen 1s peak had been detected in the XPS spectra, although the concentration of N ions was not determined) in Ref. [37,38]. There are two main reasons for film doping: first, to extend the light absorption interval toward the visible spectrum, with a purpose to increase the efficiency of solar-light photocatalysis. The second is to create trapping centres for electron-hole pairs in order to prolong their lifetime before recombination. Except [24,26], where Na entered the film by thermal diffusion from the substrate (soda lime glass), the samples were especially doped by various techniques. The dopant concentrations shown in brackets are the values presented in the respective papers and determined by XPS analysis. The authors of these papers concluded that doping of TiO_2 thin films is favourable for the photocatalytic activity in some cases.

According to the LIMS analysis (Table 2) the concentrations of C, Na, Fe and Cu are all of the same order of magnitude (~0.1 at.%). However, as was already mentioned in Section 3.4, only carbon was detected by XPS in all samples, with additional traces of Na and Zn found in samples 30 and 31 only. This means that the spatial distribution of metallic impurities is very different from that of carbon, and that the surface concentrations of these elements are below the detection limit of XPS. As to the sample 30 for which both the photocatalytic activity and the XPS spectra were studied, we may assume that according to Refs. [24,26], the presence of Na can slightly decrease the photocatalytic activity (note that the concentration of Na in the sample 30 is much lower than those used in Refs. [24,26]).

Of all the commercial sources of TiO_2, the Degussa P25 powder has become widely recognised as the golden standard,

due to its high specific surface area (about 50 m^2/g) and the resulting high activity [13]. The photocatalytic performance of the Degussa P25 powder of the same weight deposited on the glass is markedly better than that of the CVD films (Table 4). We should, however, take into account the difference in the specific area of the CVD thin films and those deposited from suspensions of the Degussa powder. The CVD films grown for this study had a good transparency to the eye. AFM images revealed film crystallites of about 100 nm in diameter. Therefore, following Ref. [12], we may presume the electrode specific surface area is not very different from the geometric area (7.85×10^{-3} m^2). Meanwhile, a suspension of 7 mg (the typical mass of a CVD film) of the Degussa P25 powder in water has the surface area of ca. 0.35 m^2, assuming well-separated microcrystals. It is clear, however, that the powder deposited on the glass substrate does not constitute such a large specific surface area for the photocatalytic purposes. The reason is that only a half of the TiO_2 particle, oriented toward the light source, can be directly illuminated by the UV light. Another factor that reduces the effective specific surface area is the agglomeration of powder particles. The lower limit of the effective surface area is the geometric area of the film.

A recent discussion had been devoted to the photocatalytic properties of the two polycrystalline TiO_2 phases—anatase and rutile. In general, it is assumed that the crystallite size is larger for rutile, its catalytic activity, however, is lower as compared to the anatase form. The difference in the lattice structure causes different mass densities and electronic band structures of the two TiO_2 forms. As a result, the band gap increases and the band edges shifts to larger redox potentials, making the anatase form of TiO_2 a much better catalyst than the rutile form.

The problem of the rutile 110 surface activity was recently studied both experimentally and theoretically. Based on the experimental results, it has been variously proposed that water (a) adsorbs molecularly on the 110 surface and only dissociates at defect sites [39], (b) adsorbs dissociatively at low coverages and thereafter molecularly [40], (c) adsorbs either molecularly or dissociatively depending on temperature [41]. One point of consensus is that if dissociation does occur, it only occurs at low concentrations. It was recently calculated [42] using the first principles density-functional method that a monolayer of H_2O on the rutile 110 surface would contain water in both molecular and dissociated forms. Based on these results, it is possible to conclude that the 110 surface should be photocatalytically active. The CVD thin films annealed at high temperatures had been shown to have the 110 crystal orientation [15], thus we can expect the same 110 termination to be present in the films prepared at lower temperatures.

Considering Fig. 10, we conclude that there operate at least two different mechanisms of photodegradation of Fenarimol. Considering that the films prepared from precursor A have shown no evidence of the photocatalytic activity (see Table 4), the catalytic effect was attributed to the anatase phase of the samples prepared from precursor B.

A possible explanation of these different photocatalytic properties of anatase and rutile can be derived from the recent developments in the photo-induced transient charge separation [20]. The optical bandgap E_g values, derived from extrapolation of the absorption coefficients of oriented thin films of anatase and rutile forms, are 3.23 and 3.02 eV, respectively. The threshold energies of the photoconductivity spectra were found to agree well with the optical bandgap values [20]. These values are in fact quite close for the two forms of titania. The parameter that does make a large difference between the two forms is the charge separation efficiency of the photogenerated electrons and holes in the wavelength range of 340–380 nm [20], which is significantly higher for the anatase films.

4. Conclusions

The physical and photocatalytical properties of thin films prepared by CVD from two different precursors, titanium[(dipiraloymethanate) diisopropoxide] $Ti(dpm)_2(OPr^i)_2$ and titanium[isopropoxide] $Ti(OPr^i)_4$ were discussed. It was demonstrated that the photoassisted CVD method can be implemented for thin film synthesis using the $Ti(dpm)_2(OPr^i)_2$ precursor and high-pressure mercury lamps as a UV light source. Two different crystalline forms, rutile and anatase, could be prepared using these precursors, as demonstrated by XRD. LIMS and XPS analyses revealed that surface composition is different from that of the bulk of the film. The structure of the TiO_2 thin film photocatalysts has a dominating effect on the photodegradation rate of the Fenarimol test compound.

Acknowledgements

The authors are grateful to Fundação para a Ciência e Tecnologia for the financial support given in the framework of the projects POCTI/43520/FIS/2000, 423/DAAD-ICCTI and project II-01-64 (HASYLAB) and to Degussa Portugal for the TiO_2 powder gift. This work was supported by the European Community-Research Infrastructure Action under the FP6 "Structuring the European Research Area" Programme (through the Integrated Infrastructure Initiative "Integrating Activity on Synchrotron and Free Electron Laser Science") in the framework of IHP-Contract HPRI-CT-1999-00040/2001-00140.

References

[1] K. Honda, A. Fujishima, Nature 238 (1972) 37.
[2] W.W. Xu, R. Kershaw, K. Dwight, A. Wold, Mater. Res. Bull. 25 (1990) 1385.
[3] M.O. Abou-Helal, W.T. Seeber, Appl. Surf. Sci. 195 (2002) 53.
[4] B.G. Dixon, M.A. Wals, P.G. Phillips, R.S. Morris, J. Mater. Res. 10 (1995) 2626.
[5] J. Yu, X. Zhao, O. Zhao, Mater. Chem. Phys. 69 (2001) 25.
[6] S.K. Zheng, T.M. Wang, G. Xiang, C. Wang, Vacuum 62 (2001) 361.
[7] D. Dumitriu, A.R. Bally, C. Ballif, P. Hones, P.E. Schmid, R. Sanjines, F. Lévy, V.I. Pârvulescu, Appl. Catal., B Environ. 25 (2000) 83.
[8] S.-H. Lee, M. Kang, S.M. Cho, G.Y. Han, B.-W. Kim, K.J. Yoon, C.-H. Chung, J. Photochem. Photobiol., A Chem. 146 (2001) 121.

[9] R. Paily, A. DasGupta, N. DasGupta, P. Bhattacharya, P. Mista, T. Ganguli, L.M. Kukreja, A.K. Balamurugan, S. Rajagopalan, A.K. Tyagi, Appl. Surf. Sci. 187 (2002) 297.
[10] J. Aarik, A. Aidla, T. Uustare, K. Kukli, V. Sammelselg, M. Ritala, M. Leskelä, Appl. Surf. Sci. 193 (2002) 277.
[11] D. Byun, Y. Jin, B. Kim, J.K. Lee, D. Park, J. Hazard. Mater. B 73 (2000) 199.
[12] M.L. Hitchman, F. Tian, J. Electroanal. Chem. 538-539 (2002) 165.
[13] A. Mills, N. Elliot, I.P. Parkin, S.A. O'Neill, R.J. Clark, J. Photochem. Photobiol., A Chem. 151 (2002) 171.
[14] V.G. Bessergenev, I.V. Khmelinskii, R.J.F. Pereira, V.V. Krisuk, A.E. Turgambaeva, I.K. Igumenov, Vacuum 64 (2002) 275.
[15] V.G. Bessergenev, R.J.F. Pereira, M.C. Mateus, I.V. Khmelinskii, E. Burkel, R.C. Nicula, Int. J. Photoenergy 5 (2003) 99.
[16] N. Kaliwoh, J.-Y. Zhang, I.W. Boyd, Appl. Surf. Sci. 186 (2002) 241.
[17] A. Hagen, A. Barkschat, J.K. Dohrmann, H. Tributsch, Sol. Energy Mater. Sol. Cells 77 (2003) 1.
[18] D.M. Adams, Inorganic Solids, J. Wiley & Sons, U.S.A., 1974, p. 72.
[19] A. Sclafani, L. Palmisano, M. Schiavello, J. Phys. Chem. 94 (1990) 829.
[20] T. Sumita, T. Yamaki, S. Yamamoto, A. Miyashita, Appl. Surf. Sci. 200 (2002) 21.
[21] V.V. Krisyk, A.E. Turgambaeva, I.K. Igumenov, V.G. Bessergenev, I.V. Khmelinskii, R.J.F. Pereira, Proceedings of the XVth International Symposium on CVD, Toronto, Canada, May 4–6,2000, p. 284.
[22] S.P. Krumdieck, R. Rai, Chem. Vap. Depos. 7 (2001) 85.
[23] R. Nicula, M. Stir, C. Schick, E. Burkel, Thermochim. Acta 403/1 (2003) 129.
[24] J.C. Yu, H.Y. Tang, J. Yu, H.C. Chan, L. Zhang, Y. Xie, H. Wang, S.P. Wong, J. Photochem. Photobiol. 153 (2002) 211.
[25] J. Yu, X. Zhao, Mater. Res. Bull. 35 (2000) 1293.
[26] J. Yu, X. Zhao, Mater. Res. Bull 36 (2001) 97.
[27] K. Baba, R. Hatada, Surf. Coat. Technol. 136 (2001) 241.
[28] L. Li, W. Zhu, P. Zhang, Z. Chen, W. Han, Water Res. 37 (2003) 3646.
[29] A. Jitianu, T. Cacciaguerra, R. Benoit, S. Delpeux, F. Bégun, S. Bonnamy, Carbon 42 (2004) 1147.
[30] S.E. Park, H. Joo, Joon W. Kang, Sol. Energy Mater. Sol. Cells 83 (2004) 39.
[31] H. Yamashita, M. Harada, J. Misaka, H. Nakao, M. Takeuchi, M. Aupo, Nucl. Instrum. Methods Phys. Res., Sect. B 206 (2003) 889.
[32] S.K. Zheng, T.M. Wang, W.C. Hao, R. Shen, Vacuum 65 (2002) 155.
[33] C. Wang, T. Wang, S. Zheng, Physica, E 14 (2002) 242.
[34] I.M. Arabatzis, T. Stergiopoulos, D. Andreeva, S. Kitova, S.G. Neophytides, P. Falaras, J. Catal. 220 (2003) 127.
[35] S.K. Zheng, T.M. Wang, C. Wang, G. Xiang, Nucl. Instrum. Methods Phys. Res., Sect. B 187 (2002) 479.
[36] M. Aupo, M. Takeuchi, J. Catal. 216 (2003) 505.
[37] Y. Suda, H. Kawasaki, T. Ueda, T. Oshima, Thin Solid Films 453–454 (2004) 162.
[38] L. Miao, S. Tanemura, H. Watanabe, Y. Mori, K. Kaneko, S. Toh, J. Cryst. Growth 260 (2004) 118.
[39] M.A. Henderson, Surf. Sci. 355 (1996) 151.
[40] M.B. Hugenschmidt, L. Gamble, C.T. Cambell, Surf. Sci. 302 (1994) 329.
[41] R.L. Kurtz, R. Stockbaumer, T.E. Madey, E. Roman, J.L. Segovia, Surf. Sci. 218 (1989) 178.
[42] P.J. Dlindan, N.M. Harrison, M.J. Gillian, Phys. Rev. Lett. 80 (1998) 762.
[43] M.C.D.A. Mateus, A.M. Silva, H. Burrows, Chemosphere 48 (2002) 363.
[44] Powder Diffraction Fail, Joint Committee on Powder Diffraction Standards, ASTM, Philadelphia, PA, 1967, Card 89-4920.
[45] Powder Diffraction Fail, Joint Committee on Powder Diffraction Standards, ASTM, Philadelphia, PA, 1967, Card 89-421.